StAR-related lipid transfer domain 11 (STARD11)–mediated ceramide transport mediates extracellular vesicle biogenesis

Received for publication, February 22, 2018, and in revised form, August 17, 2018 Published, Papers in Press, August 23, 2018, DOI 10.1074/jbc.RA118.002587

Masanori Fukushima[‡§1], **Debanjali Dasgupta**[‡], **Amy S. Mauer**[‡], **Eiji Kakazu**[‡2], **Kazuhiko Nakao**[§], and **Harmeet Malhi**[‡3]

From the [‡]*Division of Gastroenterology and Hepatology, Mayo Clinic, Rochester, Minnesota 55905 and the* [§]*Department of Gastroenterology and Hepatology, Nagasaki University Graduate School of Biomedical Sciences, Nagasaki 852-8501, Japan*

Edited by Phyllis I. Hanson

Extracellular vesicles are important carriers of cellular materials and have critical roles in cell-to-cell communication in both health and disease. Ceramides are implicated in extracellular vesicle biogenesis, yet the cellular machinery that mediates the formation of ceramide-enriched extracellular vesicles remains unknown. We demonstrate here that the ceramide transport protein StAR-related lipid transfer domain 11 (STARD11) mediates the release of palmitate-stimulated extracellular vesicles having features consistent with exosomes. Using palmitate as a model of lipotoxic diseases and as a substrate for ceramide biosynthesis in human and murine liver cell lines and primary mouse hepatocytes, we found that STARD11-deficient cells release fewer extracellular vesicles. Moreover, STARD11 reciprocally regulated exosome ceramide enrichment and cellular ceramide depletion. We further observed that in STARD11 knockout cells intracellular ceramide accumulates and that this apparent inability to transfer cellular ceramide into extracellular vesicles reduces cellular viability. Using endogenous markers, we uncovered structural and functional colocalization of the endoplasmic reticulum (ER), STARD11, and multivesicular bodies. This colocalization increased following palmitate treatment, suggesting a functional association that may mediate ceramide trafficking from the ER to the multivesicular body. However, the size and number of multivesicular bodies were comparable in WT and STARD11-knockout cells. In conclusion, we propose a model of how STARD11 mediates ceramide trafficking in palmitate-treated cells and stimulates exosome biogenesis.

Extracellular vesicles are an important carrier of cell-derived information with emerging roles in cell-to-cell communication in health and disease (1–4). Extracellular vesicles can be classified into exosomes, which arise from the multivesicular body, microvesicles derived from the plasma membrane, and apoptotic bodies formed by dying cells (5). Ceramides are known to play a role, in particular, in the formation of multivesicular body-derived exosomes (6). We have recently demonstrated that palmitate, a saturated fatty acid, elevated in the liver and in the circulation in obesity-associated disorders including fatty liver disease, stimulates the release of extracellular vesicles (7, 8). Palmitate-stimulated extracellular vesicles are enriched in ceramide, and their release depends on the *de novo* synthesis of ceramide from exogenously supplied palmitate (8). *De novo* ceramide synthesis occurs at the endoplasmic reticulum (ER)[4] (9), and exosomes are formed as intraluminal vesicles (ILVs) of the multivesicular body (MVB) (10). However, it is not known how palmitate-stimulated ceramide is transported from the ER to the MVB to form ILVs, which give rise to exosomes upon their release from cells.

Ubiquitin-dependent cargo sorting of proteins to form ILVs requires the endosomal sorting complex required for transport (ESCRT) machinery, such that RNA silencing of ESCRT machinery components yields fewer and morphologically abnormal MVBs; yet the formation of ILVs and MVBs is not fully inhibited, indicating that ILVs can be generated by cellular processes in addition to the ESCRT machinery (11). For example, the sorting of other cargoes, such as the melanosomal protein Pmel17, remains unaffected in the absence of ESCRT components (12). Furthermore, lipids are also implicated in the formation of ILVs. The phospholipid lysobisphosphatidic acid can induce the formation of multivesicular liposomes in cell-free systems that resemble the MVB; although this lipid is found *in vivo*, its role in the formation of ILVs remains unexplored (13, 32). The sphingolipid ceramide is implicated in

This work was supported by National Institutes of Health Grant DK111378 (to H. M.), by Gilead Sciences Research Scholars Program in Liver Disease, by the Palumbo Foundation, and by the Strickland Career Development Award (to H. M.). The authors declare that they have no conflicts of interest with the contents of this article. The content is solely the responsibility of the authors and does not necessarily represent the official views of the National Institutes of Health.

This article contains Figs. S1–S3.

[1] Present address: Dept. of Gastroenterology and Hepatology, Nagasaki University Graduate School of Biomedical Sciences, 1-7-1 Sakamoto, Nagasaki 852-8501, Japan.

[2] Present address: Division of Gastroenterology, Tohoku University Hospital, 1-1 Seiryo-machi, Aoba-ku, Sendai City, Miyagi 980-8574, Japan.

[3] To whom correspondence should be addressed: Mayo Clinic, 200 First St. SW, Rochester, MN 55905. Tel.: 507-284-0686; Fax: 507-284-0762; E-mail: malhi.harmeet@mayo.edu.

[4] The abbreviations used are: ER, endoplasmic reticulum; CERT, ceramide transport protein; ESCRT, endosomal sorting complex required for transport; EV, extracellular vesicle; FFAT, diphenylalanines in an acidic tract; ILV, intraluminal vesicle; IMH, immortalized mouse hepatocyte; MVB, multivesicular body; N-Rh-PE, N-lissamine rhodamine B 1,2-dihexadecanoyl-*sn*-glycero-3-phosphoethanolamine; OA, oleate; PA, palmitate; STARD, StAR-related lipid transfer domain; TSG101, tumor susceptibility gene 101; VAP, vesicle-associated membrane protein-associated protein; FMK, fluoromethyl ketone; PDI, protein disulfide isomerase; DMEM, Dulbecco's modified Eagle's medium; FBS, fetal bovine serum.

the formation of ILVs and release of exosomes, such that inhibition of ceramide biosynthesis decreases exosome release (6, 8). Thus, accumulated observations indicate that MVB biogenesis is diverse, and multiple mechanisms contribute to cargo packaging into the ILVs of MVBs and their release as exosomes.

The *de novo* biosynthesis of ceramide occurs at the ER (9). Newly formed ceramide is transported from the ER to the Golgi by nonvesicular transport mediated by ceramide transport protein (CERT), also known as StAR-related lipid transfer domain (STARD) 11, an evolutionarily conserved member of the STARD family of lipid transporting proteins with high substrate specificity (14–17). The role of STARD11 in the formation of exosomes that are formed in a ceramide-dependent manner remains unknown.

Lipotoxicity of the saturated free fatty acid palmitate is a robust model for examining signaling pathways activated in lipotoxic hepatocytes, a cellular model germane to nonalcoholic fatty liver disease (19). In this regard, we have previously demonstrated that palmitate treatment leads to the release of extracellular vesicles from hepatocytes and that significant extracellular vesicle release occurs before the onset of palmitate-induced apoptosis (8). Furthermore, we have demonstrated that these vesicles are enriched in ceramide and dependent on the *de novo* synthesis of ceramide. However, the cellular trafficking machinery that mediates ceramide transport to form extracellular vesicles remains unknown. Herein, we report that in the absence of STARD11, palmitate-induced extracellular vesicle release is attenuated; correspondingly, when cells are unable to release ceramide containing extracellular vesicles, intracellular ceramide content increases with deleterious consequences. Palmitate-stimulated extracellular vesicles display markers consistent with exosomes. We demonstrate structural and functional colocalization of the ER, STARD11, and the MVB; this colocalization is increased by palmitate treatment. Thus, we have demonstrated that the ceramide transport protein STARD11 mediates the release of lipotoxic extracellular vesicles, likely via transport of newly synthesized ceramide from the ER to the MVB.

Results

STARD11 is expressed in hepatocytes and mediates palmitate-induced extracellular vesicle release

Prolonged palmitate treatment induces hepatocyte apoptosis (19, 20); therefore, we designed our experimental conditions to collect conditioned media for extracellular vesicle isolation following 16 h of treatment prior to the onset of significant palmitate-induced apoptosis, which occurred following 24 h of palmitate treatment as measured biochemically by caspase 3/7 activity (Fig. S1*A*). Moreover, we confirmed that palmitate-induced extracellular vesicle release was preserved in the presence of the caspase inhibitors benzyloxycarbonyl-VAD-FMK and IDN-6556 (Fig. S1*B*) and thus was not due to apoptotic bodies, which cannot be formed in the presence of caspase inhibitors (21). We further excluded a contribution from protein aggregates to palmitate-stimulated extracellular vesicles by floating extracellular vesicles in an iodixanol gradient, as previously described by Kowal *et al.* (22). Palmitate-stimulated extracellular vesicles were isolated from fractions 3, 5, and 6 (Fig. S1*C*).

Having established conditions for extracellular vesicle isolation, we next probed the hepatocyte expression of STARD11 in human and murine hepatocellular cell lines and primary mouse hepatocytes. STARD11 protein and mRNA were easily detected in human hepatoma cell lines HepG2 and Huh7, immortalized mouse hepatocytes (IMHs), mouse hepatoma cell line Hepa1–6, and primary mouse hepatocytes (Fig. S1, *D–F*). To determine the biologic significance of STARD11 in the release of palmitate-stimulated extracellular vesicles, also referred to as lipotoxic extracellular vesicles, we asked whether the release of these lipotoxic extracellular vesicles was mediated by STARD11. We used CRISPR/Cas9 genome editing technology to knock out STARD11 in mouse and human hepatocellular cell lines. Using these STARD11 knockout cell lines (STARD11$^{-/-}$), we found that the release of lipotoxic extracellular vesicles depended on STARD11 in mouse and human hepatocytes (Fig. 1, *A* and *B*, respectively), in several distinct knockout clones. We verified the deletion of STARD11 by Western blotting (Fig. 1, *A* and *B*, *bottom panels*). Lipid loading can stimulate lipoprotein secretion; therefore, we interrogated our cell line for apolipoproteins A1, B100, and B48, which are requisite for the secretion of HDL and VLDL particles, respectively. We could not detect these lipoproteins in our cell line and in palmitate-stimulated extracellular vesicles excluding a contribution of coisolated HDL particles and VLDL particles to our extracellular vesicle counts (Fig. S1*G*).

Oleate, a monounsaturated fatty acid, is the second most physiologically abundant fatty acid in humans (7). Unlike palmitate, oleate is not a direct substrate for the formation of ceramides (23). Therefore, we asked whether oleate treatment led to extracellular vesicle release. We found no increase in extracellular vesicle release in oleate treated WT cells and similar responses in STARD11$^{-/-}$ cells (Fig. 1, *A* and *B*). Thus, STARD11 is requisite for the release of palmitate-stimulated lipotoxic extracellular vesicles. We did not observe any changes in the size distribution of extracellular vesicles from STARD11$^{-/-}$ cells compared with WT cells in either mouse or human hepatocytes (Fig. 1, *C* and *D*). We next analyzed basal extracellular vesicle release in control and STARD11$^{-/-}$ cells. We found that basal extracellular vesicle release was comparable in WT and STARD11$^{-/-}$ mouse (Fig. 1*E*) and human (Fig. 1*F*) hepatocytes. Altogether these data demonstrate that STARD11 mediates extracellular vesicle release specifically following palmitate treatment. This is likely due to *de novo* synthesis of ceramide from palmitate, as previously reported by us (8), and possibly due to the trafficking of palmitate-stimulated ceramide to the MVB.

Extracellular vesicle and whole-cell ceramide are reciprocally related in STARD11 knockout cells

Because the release of palmitate-stimulated extracellular vesicles depends on ceramide biosynthesis as previously shown by us (8) and confirmed (Fig. S2*A*), we asked whether a defect in ceramide transport affects extracellular vesicle-ceramide content. We reasoned that extracellular vesicles derived from WT

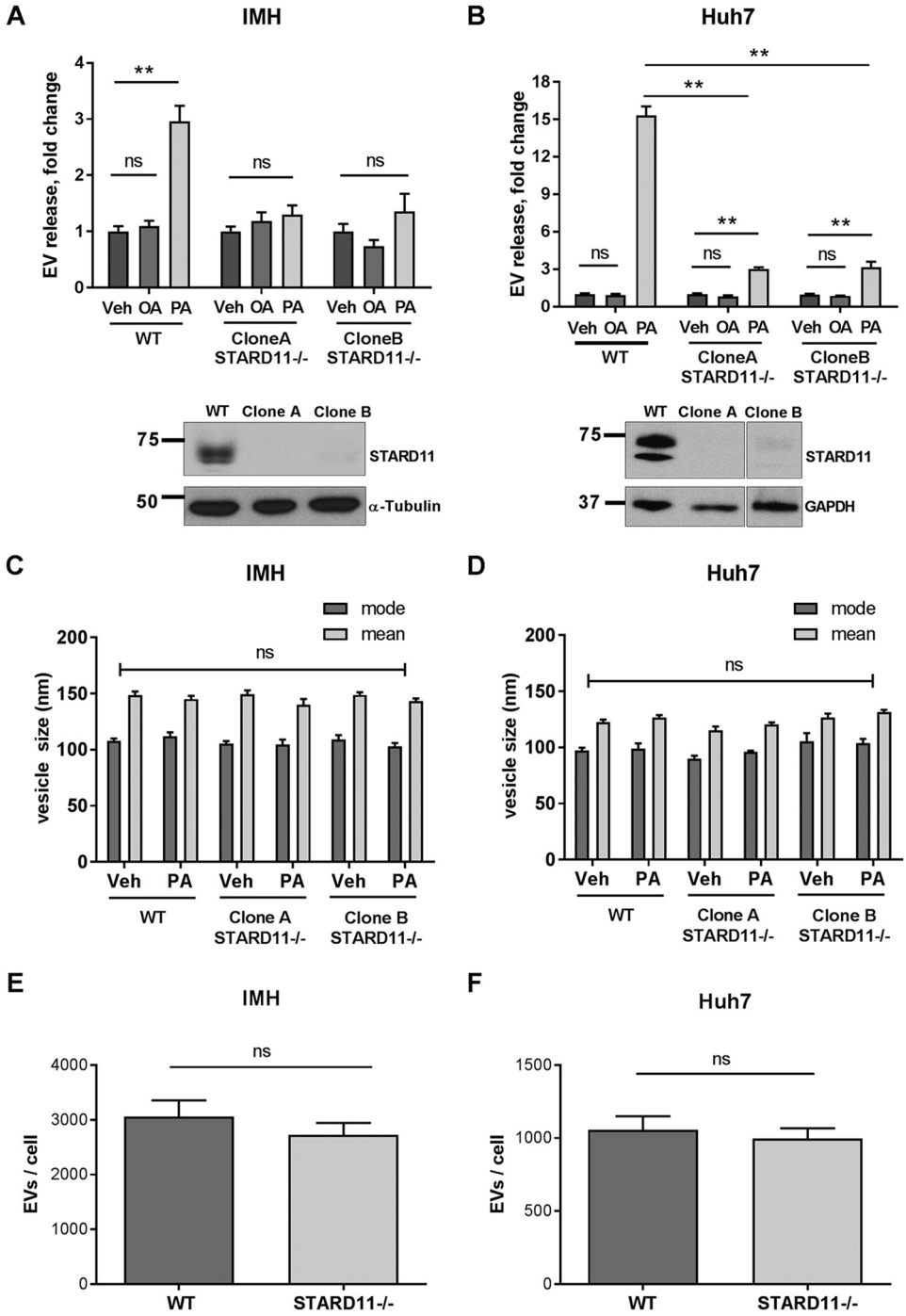

Figure 1. Palmitate-induced EV release is STARD11-dependent. *A*, EV release in IMH cell line from WT and two STARD11 knockout (STARD11$^{-/-}$) clones treated with vehicle (*Veh*) or 400 μM OA or PA, each for 16 h. The Western blots in the *bottom panel* confirm the deletion of STARD11 in both clone A and clone B. *B*, EV release in human hepatocyte cell line, Huh7, WT, and STARD11$^{-/-}$ clones treated with vehicle or 400 μM OA or PA, each for 16 h. The Western blots confirm the deletion of STARD11 in both clone A and clone B. *C* and *D*, size of EVs from IMH and Huh7 WT and STARD11$^{-/-}$ cells measured by nanoparticle tracking analysis. *E* and *F*, basal EV release per cell in WT and STARD11$^{-/-}$ IMH and Huh7 cells. **, $p < 0.01$; *ns*, not significant. All *error bars* are S.E. These data were obtained from three or more independent experiments.

cells would be ceramide-enriched, whereas extracellular vesicles derived from STARD11$^{-/-}$ cells, which lack ceramide transport protein, would not. To demonstrate that STARD11 is required for the biosynthesis of ceramide-enriched extracellular vesicles, we measured extracellular vesicle ceramide by tandem MS. Consistent with our previous data (8), palmitate treatment led to the release of ceramide-enriched extracellular vesicles (Fig. 2*A*). However, extracellular vesicles derived from palmitate-treated STARD11$^{-/-}$ cells were not enriched in ceramide. We found no increase in ceramide in oleate-stimulated extracellular vesicles (Fig. 2*B*). Palmitate treatment led to an increase in whole-cell ceramide in WT cells (Fig. 2*C*). The increase in whole-cell ceramide levels was significantly greater in STARD11$^{-/-}$ cells (Fig. 2*C*). Oleate treatment did not increase whole-cell ceramide levels in WT or STARD11$^{-/-}$ cells (Fig. 2*D*). These data suggest that

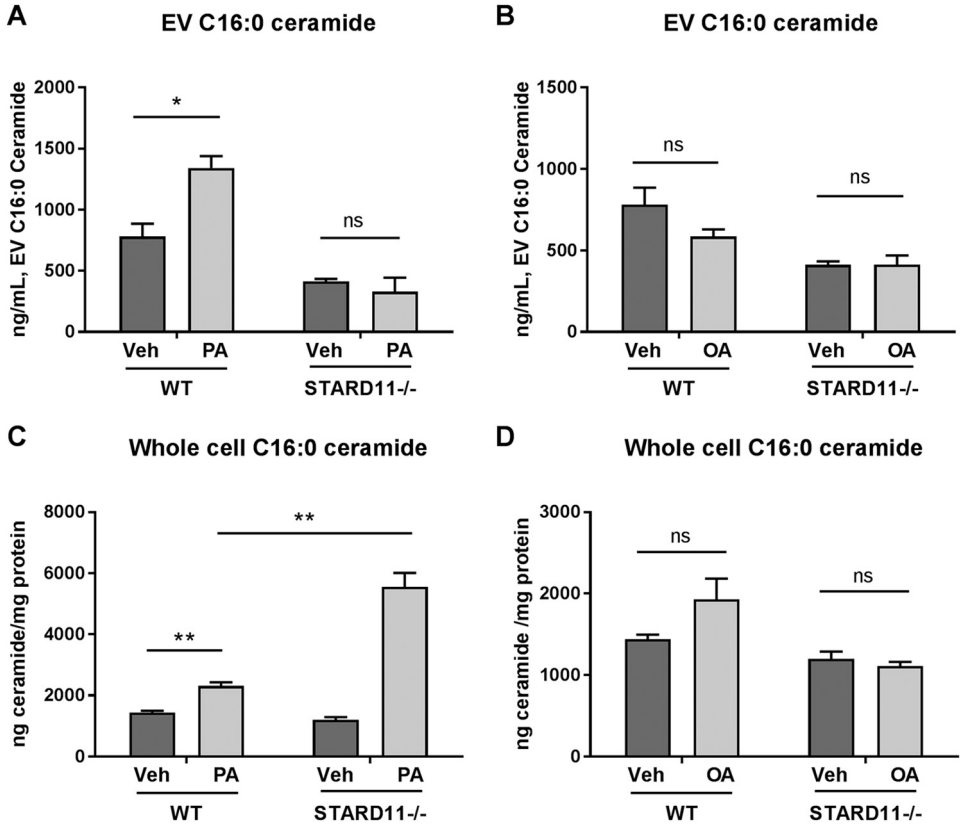

Figure 2. EV ceramide enrichment is STARD11-dependent. *A* and *B*, EVs were isolated from immortalized mouse hepatocyte cell line from WT and STARD11 knockout (STARD11$^{-/-}$) cells treated with vehicle (*Veh*) or 400 μM PA or OA for 16 h. The C16:0 ceramide content of EVs was measured by LC–MS/MS. *C* and *D*, the C16:0 ceramide was measured in whole-cell pellets under the same condition as above and normalized to protein content. *, $p < 0.05$; **, $p < 0.01$; *ns*, not significant. All *error bars* are S.E. These data were obtained from three or more independent experiments.

STARD11-mediated trafficking of palmitate-stimulated ceramide is an important pathway for the cellular export of ceramide because STARD11$^{-/-}$ cells accumulate ceramide intracellularly.

STARD11-mediated ceramide transport mitigates palmitate-induced cytotoxicity

Having demonstrated ceramide accumulation in STARD11$^{-/-}$ cells, we next asked whether ceramide accumulation is toxic for cells. As discussed above, we found no increase in cell death or decrease in cell viability following 16 h of treatment with palmitate to correspond to the time that conditioned medium was collected for extracellular vesicle isolation. However, a longer duration of palmitate treatment led to a greater increase in cell death and a reduction in cell viability in STARD11$^{-/-}$ cells compared with WT cells following 20 h of palmitate treatment, consistent with our previous publications, which have demonstrated a significant time dependence of palmitate-induced hepatocyte apoptosis (Fig. S2, *B* and *C*) (19, 20). These data suggest that the ability to exclude ceramide from hepatocytes partially mitigates palmitate-induced toxicity.

Palmitate-stimulated extracellular vesicles have features of exosomes

Small extracellular vesicles derived from multivesicular bodies are known to express an array of markers, suggestive of their cellular origin within the MVB (22, 24). These markers include Alix, syntenin, and tumor susceptibility gene 101 (TSG101), which have been demonstrated to be markers of small extracellular vesicles arising from the MVB, *i.e.* exosomes (22, 24). We interrogated palmitate-stimulated EVs for the presence of Alix, syntenin, and TSG101 and found that these markers were enriched in palmitate-stimulated extracellular vesicles from WT cells, suggesting that these extracellular vesicles are exosomes arising within the MVB (Fig. 3). In STARD11$^{-/-}$ cells, basal levels of Alix, syntenin, and TSG101 were comparable with WT cells, and there was no increase in these exosome markers following palmitate treatment. We also observed an increase in CD81 in extracellular vesicles from palmitate-treated WT cells and not in STARD11$^{-/-}$ cells. Whole-cell levels of Alix, syntenin, and TSG101 were unchanged following palmitate treatment.

STARD11 is a membrane-bound protein that is known to bind with vesicle-associated membrane protein-associated protein (VAP) in the ER membrane with its FFAT motif and phosphatidylinositol-4 monophosphate in the Golgi membrane with its N-terminal pleckstrin homology domain (25, 26). However, it is known to also bind phosphatidylinositol-3 monophosphate, which is enriched in endosome membranes (27). In this location, it could be internalized as a component of the ILV membrane. To address this question, we first asked whether STARD11 is a part of the extracellular vesicle cargo. As demonstrated in the Western blotting analysis, we did not

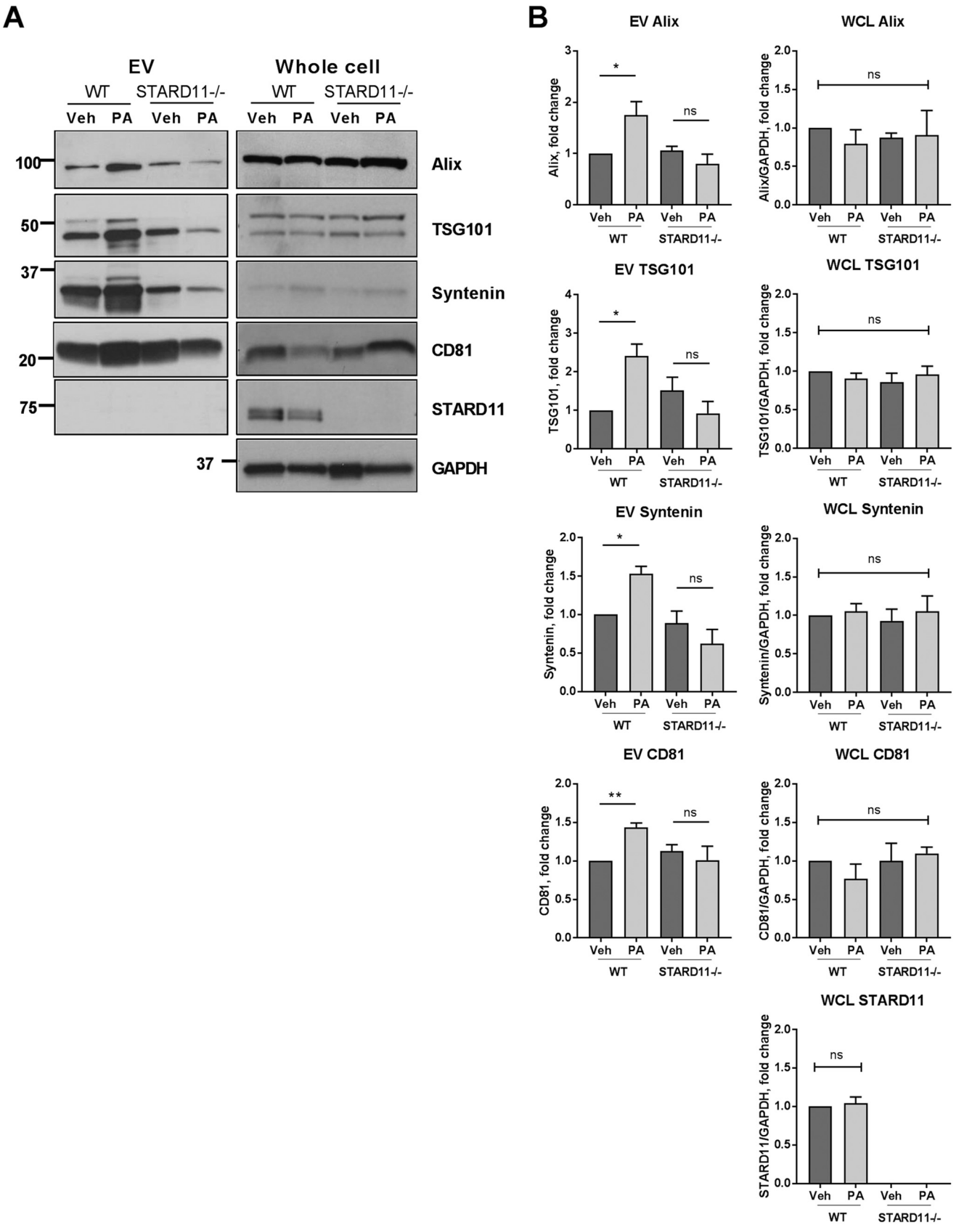

Figure 3. Palmitate-stimulated EVs are consistent with exosomes. *A*, EVs isolated from equal number of cells and whole-cell lysates (*WCL*) from immortalized mouse hepatocyte cell line were analyzed by Western blotting. Alix, TSG101, syntenin, and CD81 were used as small EV markers. GAPDH was used as a loading control. *B*, these expression levels were quantified by densitometry. *, $p < 0.05$; **, $p < 0.01$; *ns*, not significant; *Veh*, vehicle. All *error bars* are S.E. These data were obtained from three or more independent experiments.

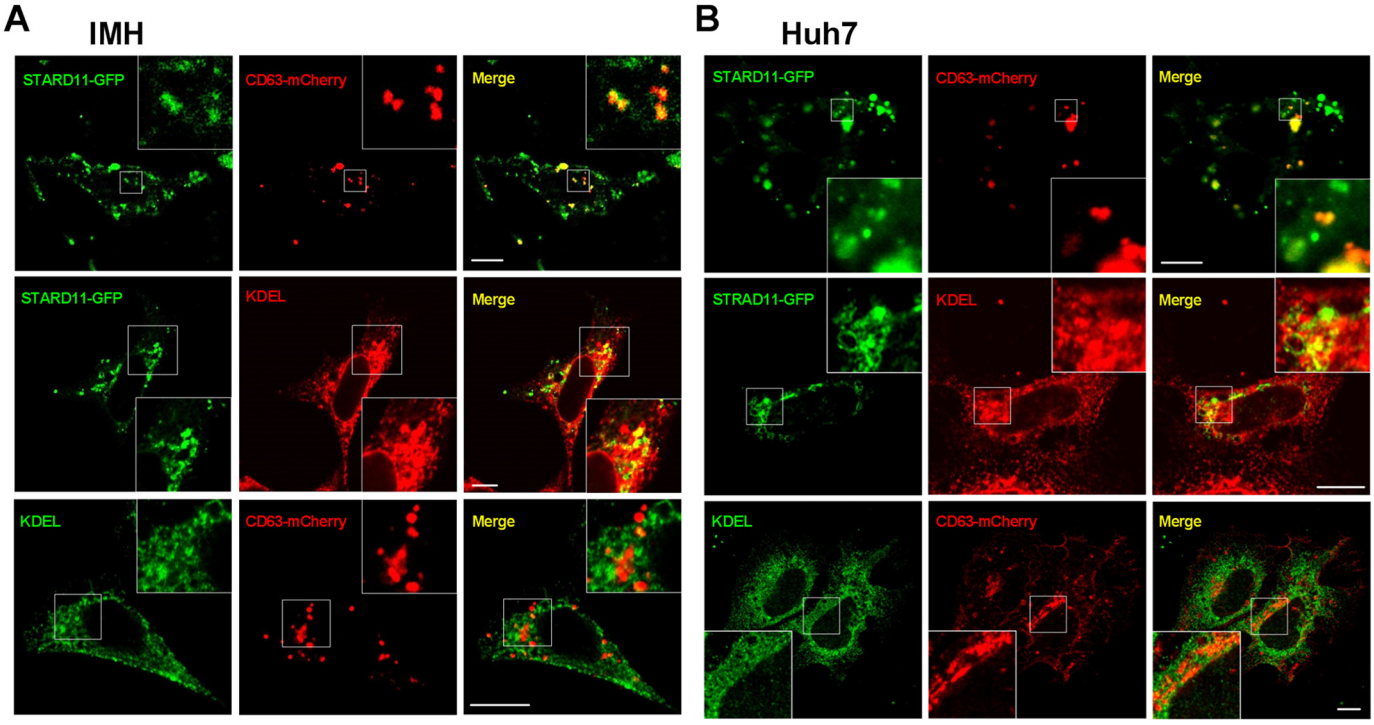

Figure 4. STARD11 is colocalized with ER and MVB. *A* and *B*, IMH (*A*) and Huh7 (*B*) were cotransfected with GFP-tagged STARD11 and mCherry-tagged CD63 to label MVB (*top panels*). The cells were transfected with GFP tagged-STARD11 and were then labeled with anti-KDEL antibody by immunofluorescence for ER marker (*middle panels*). The cells were transfected with mCherry-tagged CD63 and were then labeled with anti-KDEL antibody by immunofluorescence (*bottom panels*). The *insets* depict a higher magnification of the selected region. The *scale bar* indicates 10 μm.

detect STARD11 on isolated extracellular vesicles, both basally and in palmitate-stimulated extracellular vesicles (Fig. 3).

STARD11 colocalizes with ER and MVB

We asked whether STARD11 associates with the membrane compartment where ceramide synthesis occurs (the ER) and the MVB, where exosomes are formed. As previously reported by others (29), we observed MVBs within 30 nm of the ER membrane suggestive of functional colocalization (Fig. S3*A*). To confirm these observations, we used immunofluorescence microscopy in mouse hepatocyte cell line transfected with GFP-tagged STARD11 (STARD11–GFP) and CD63 tagged with mCherry (CD63–mCherry) (Fig. 4*A*). We found that STARD11 colocalized with the MVB. Next, we performed immunofluorescence for the ER marker KDEL, an ER localization motif (30), in a mouse hepatocyte cell line transfected with STARD11–GFP. We found that STARD11 colocalized with the ER. We also confirmed that the ER and MVB were in close proximity in cells transfected with CD63–mCherry to label the MVB and KDEL immunofluorescence to label the ER. We confirmed this colocalization in human hepatoma cell line, Huh7 (Fig. 4*B*).

Palmitate increases the colocalization of STARD11 with the MVB

Having demonstrated a structural colocalization between the ER, MVB, and STARD11, we next asked whether STARD11 association with the MVB increases following palmitate treatment. We first validated the specificity of the STARD11 antibody (Fig. S3*B*). Next, as demonstrated in Fig. 5 (*A* and *B*), we found that there was significant colocalization of endogenous STARD11 with the MVB, which increased significantly further following palmitate treatment (Fig. 5*B*). To confirm these findings, we utilized the fluorescent sphingolipid N-Rh-PE, which efficiently labels MVBs and has been used to study MVB trafficking (31, 32). Mouse hepatocyte cell line transfected with CD63 tagged with GFP (CD63–GFP) was labeled with N-Rh-PE. Both N-Rh-PE and CD63 labeled the same cellular compartment as demonstrated in Fig. 5*C*. Next, as demonstrated in Fig. 5 (*D* and *E*), we found that there was significant colocalization of STARD11 with the N-Rh-PE–labeled MVB, which increased significantly further following palmitate treatment. Notably, total protein and mRNA levels of STARD11 were unchanged in palmitate-treated hepatocytes (Fig. S1, *D–F*). We did not observe an increase in STARD11 and Golgi colocalization (Fig. 5, *F* and *G*). The increased association of STARD11 with MVBs following palmitate treatment demonstrates an increase in functional association between the ceramide transport protein STARD11 and the exosome formation compartment, the MVB, and likely mediates increased ceramide flux to the MVB, although we cannot exclude indirect trafficking of ceramide from the ER to the Golgi to the MVB.

To examine the association between the ER, the MVB, and STARD11 using endogenous markers, we used triple immunofluorescence microscopy in a mouse hepatocyte cell line with antibodies against protein disulfide isomerase (PDI) to label the ER, CD63 to label the endosome, and STARD11, which was detected in the cytosol and the nucleus, consistent with its known distribution. We found that STARD11 colocalized with both the ER and the MVB (Fig. 6*A*), as previously observed with

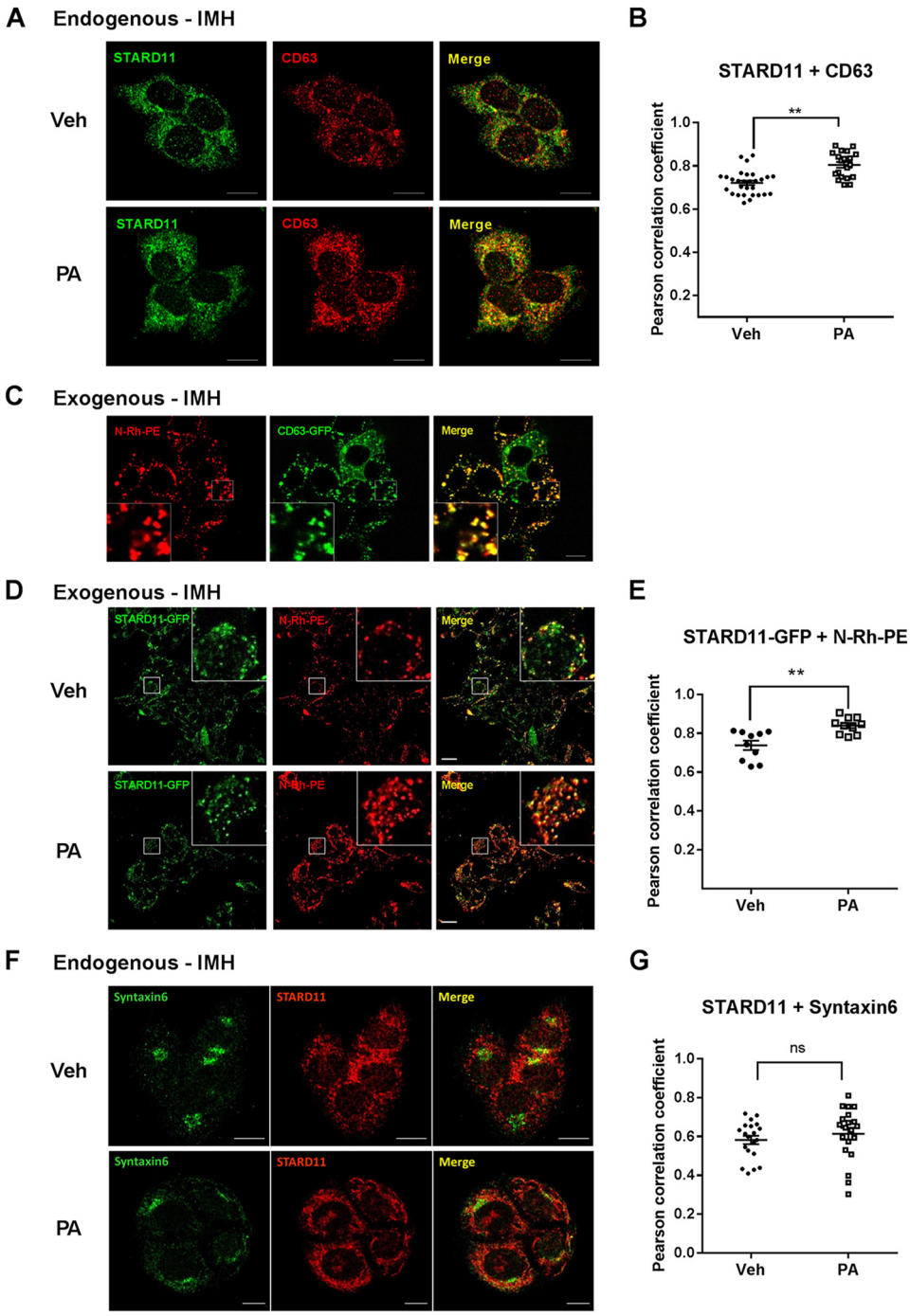

Figure 5. The colocalization of STARD11 and MVB is up-regulated by palmitate. *A*, IMH cells were treated with vehicle (*Veh*) or 300 μM PA for 1 h. After treatment, the cells were double-labeled with anti-CD63 antibody (*red*) and anti-STARD11 antibody (*green*) by immunofluorescence and observed by confocal microscopy. The *scale bar* indicates 10 μm. *B*, the Pearson correlation coefficients of colocalization between CD63 and STARD11 were analyzed by ImageJ software in 20 random fields for each condition. *C*, IMH cells were transfected with GFP-tagged CD63 and then labeled with N-Rh-PE to label MVB. The *scale bar* indicates 10 μm. *D*, IMH cells were transfected with GFP-tagged STARD11 and then labeled with N-Rh-PE. The cells were treated with vehicle or PA as above. After treatment, the cells were fixed and observed by confocal microscopy. *E*, the Pearson correlation coefficients of colocalization between STARD11–GFP and N-Rh-PE were analyzed by ImageJ software in 10 random fields for each condition. The *scale bar* indicates 20 μm. *F*, after treatment as above, IMH cells were double labeled with anti-Syntaxin6 (trans-Golgi network marker, *green*) and anti-STARD11 (*red*). *G*, the Pearson correlation coefficients of colocalization between Syntaxin6 and STARD11 were analyzed by ImageJ software in 20 random fields for each condition. The *scale bar* indicates 10 μm. **, $p < 0.01$; *ns*, not significant. All *error bars* are S.E.

the fluorescently tagged proteins. We quantified the colocalization of the endogenous markers and found that STARD11 colocalization with the MVB and ER increased following palmitate treatment as did ER and MVB colocalization (Fig. 6*B*). To further confirm *in situ* proximity between the ER and MVB, we performed a proximity ligation assay using antibodies against KDEL to label the ER and CD63 to label the MVB in palmitate-treated cells. There was a significant increase in the ER–MVB proximity as measured by the proximity ligation assay in palmitate-treated cells (Fig. 6, *C* and *D*). These colocaliza-

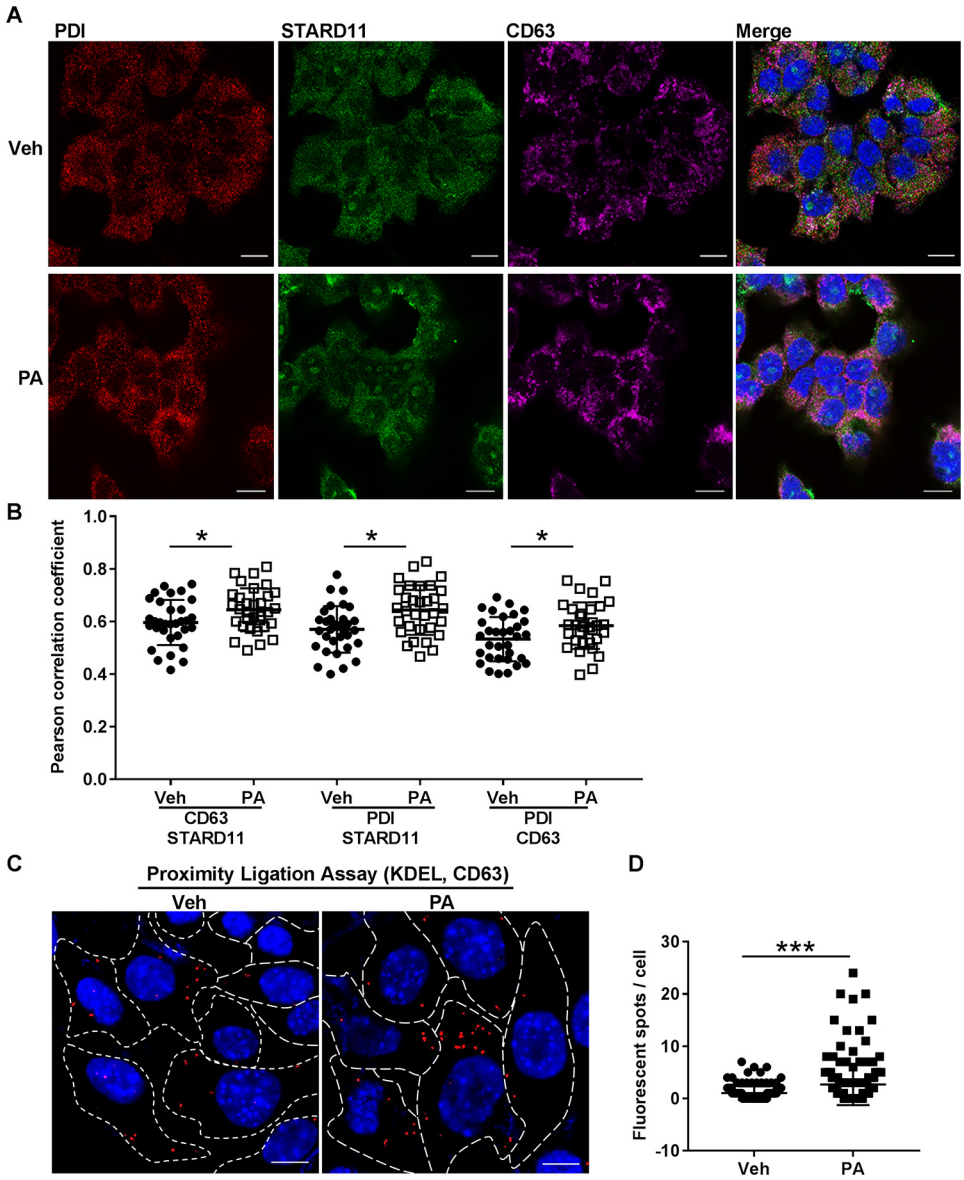

Figure 6. Palmitate up-regulates ER–MVB colocalization. *A*, IMH cells were triple-labeled with anti-PDI antibody (ER marker, *red*), anti-CD63 antibody (MVB marker, *pink*), and anti-STARD11 antibody (*green*) after treatment with vehicle (*Veh*) or 300 μM PA for 1 h. The *scale bars* indicate 10 μm. *B*, the Pearson correlation coefficients of colocalization between CD63 and STARD11, between PDI and STARD11, and between PDI and CD63 were analyzed by ImageJ software in 30 random fields for each condition. *C*, proximity ligation assay showed the interaction between anti-KDEL (ER marker) and anti-CD63 (MVB marker) antibodies as *red* fluorescent signals in IMH cells treated with vehicle or 300 μM PA. The *scale bars* indicate 10 μm. *D*, the total number of proximity ligation assay signals per cell was quantified in more than 50 cells for each condition per experiment. *, $p < 0.05$; ***, $p < 0.001$. All *error bars* are S.E. These data were obtained from three independent experiments.

tion data support an increase in functional association between the ER, STARD11, and the MVB following palmitate treatment.

MVB formation is unchanged in STARD11$^{-/-}$ cells

To determine whether an MVB formation defect in STARD11$^{-/-}$ cells is the mechanistic basis of a reduction in palmitate-induced extracellular vesicle release, we assessed MVB size and number in WT and STARD11$^{-/-}$ cells. We used the sphingolipid N-Rh-PE to label MVBs as previously described by others (32, 33) followed by super-resolution structured illumination microscopy and also EM to quantify the size and the number of MVBs. When quantified by this approach the size, morphology, and number of MVBs was unchanged between WT and STARD11$^{-/-}$ basally and following palmitate treatment (Fig. S3, *C–F*), suggesting that MVB formation is unchanged in STARD11$^{-/-}$ cells.

Processes that determine MVB trafficking into one of two fates either targeted to the plasma membrane for release or to the lysosomes for degradation remain incompletely understood. We asked whether STARD11, and hence ceramide enrichment, may contribute to endocytic trafficking. Therefore, we examined the endocytic fate of N-Rh-PE–labeled MVBs over time in live cells and focused on dissecting whether they were headed to lysosomes, labeled with LysoSensor Green. The colocalization of the MVBs and the lysosomes increased significantly in palmitate-treated STARD11$^{-/-}$ cells (Fig. 7, *A* and *B*).

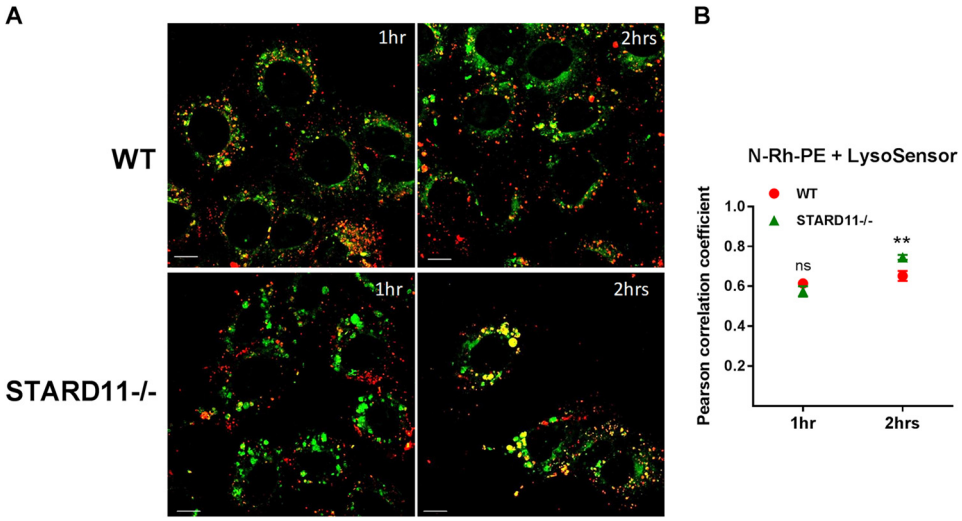

Figure 7. Palmitate treatment increases the colocalization of the MVB and lysosome in STARD11$^{-/-}$ cells. *A*, IMH WT cells and IMH-STARD11$^{-/-}$ cells were labeled with N-Rh-PE. The cells were treated with 300 μM PA for 1 or 2 h. They were also labeled with 1 μM LysoSensor Green and then fixed. *B*, the Pearson correlation coefficients of colocalization between N-Rh-PE and LysoSensor Green were analyzed in 10 random fields for each condition using ImageJ software. The *scale bar* indicates 10 μm. **, $p < 0.01$; *ns*, not significant. All *error bars* are S.E.

Discussion

Our present study describes a mechanism for the release of ceramide enriched extracellular vesicles in palmitate-treated cells, a cell-based model for hepatocyte lipotoxicity. We report that (i) STARD11 is abundant in hepatocytes; (ii) STARD11 mediates the release of palmitate-stimulated ceramide-enriched extracellular vesicles; (iii) STARD11 colocalizes to the ER and to the MVB; and (iv) STARD11-MVB colocalization and ER–MVB colocalization increases in palmitate-treated hepatocytes. These data suggest that STARD11-mediated ceramide transport to the MVB may lead to the formation of ceramide-enriched extracellular vesicles in palmitate-treated cells. Given the known physiologic role of STARD11 in transporting ceramide, which is the predominant cellular ceramide transport pathway, these data suggest that the intercompartmental transport of palmitate-stimulated ceramide by STARD11 from the ER leads to the formation of small extracellular vesicles that have features of exosomes. These data are germane to the liver lipotoxicity syndrome observed in human fatty liver disease.

STARD11 is conserved in humans and mice (34). It is a splice variant of collagen type IV α-3–binding protein (COL4A3BP) gene product lacking 26 amino acids encoded by exon 11, compared with the longer isoform, which is designated CERT$_L$. STARD11 protein contains a C-terminal START domain that mediates ceramide transport and an N-terminal pleckstrin homology domain that binds to phosphoinositide in the Golgi membrane. A middle region contains an FFAT motif that targets STARD11 to VAP on the outer surface of the ER membrane (35). Our data support a role for STARD11 in mediating ER to MVB ceramide trafficking, leading to the formation of ILVs. This may occur indirectly via trafficking to the Golgi and then to the MVB or may be a result of direct trafficking from the ER to the MVB. Although we see an increase in ER–MVB colocalization following palmitate treatment, whether truly functional membrane contact sites are formed and necessary for ceramide transport in this context is a question for future studies. We did not detect STARD11 on exosomes, suggesting that it is not an integral part of the MVB membrane. Regardless of the trafficking pathway, STARD11 mediates the release of palmitate-stimulated extracellular vesicles.

In cells that lack STARD11, we found no decrease in basal extracellular vesicle release. However, palmitate-stimulated extracellular vesicles, which have features consistent with exosomes, were reduced. Thus, we conclude that STARD11 plays a role specifically in the release of palmitate-stimulated exosome formation. Consistent with a reduction in the release of ceramide-enriched extracellular vesicles, STARD11$^{-/-}$ cells demonstrated an intracellular accumulation of ceramide that correlated with a reduction in cell viability. These data suggest that the release of ceramide via exosomes may be a pathway to mitigate palmitate-induced toxicity. As we were preparing this manuscript, Obata *et al.* (36) published a manuscript demonstrating unloading of ceramide from endothelial cells via extracellular vesicle efflux mechanisms. Given our expertise in hepatocyte lipoapoptosis (19, 20), we were careful in selecting cell culture conditions where apoptosis is not significantly increased to try to understand events that occur in viable cells. Additionally, to confirm that we were not mistaking apoptotic bodies for exosomes, we confirmed that palmitate-induced extracellular vesicle release was preserved in the presence of caspase inhibitors, which are known to inhibit the release of apoptotic bodies (21).

We found that STARD11 was abundant in human and mouse hepatocytes and mouse liver. Although levels of STARD11 did not change with lipotoxic (palmitate) treatment of cells, we noted that the compartmental distribution of STARD11 was altered in palmitate-treated cells such that there was an increase in its association with the MVB following palmitate treatment. We observed no increase in STARD11 and Golgi colocalization in palmitate-treated cells. Furthermore, we observed an increase in ER–MVB colocalization by immunofluorescence microscopy and by the proximity ligation assay in palmitate-treated cells, suggesting an increase in functional association between the ER and the MVB under palmitate

treatment. Recent studies have shown phosphorylation-dependent regulation of STARD11 contact with the ER membrane protein VAP, such that phosphorylation at serine 315 markedly enhanced STARD11-VAP interactions (37). Palmitate is a well recognized activator of the stress kinase c-Jun N-terminal kinase and other cytosolic and plasma membrane kinases (19). Whether, palmitate induces a phosphorylation-dependent increase in STARD11 interactions at the MVB is a question we will address in future experiments. We found that there were no significant decreases in MVB size and number in STARD11$^{-/-}$ cells. In conclusion, this is the first report describing the importance of the ceramide transport protein, STARD11, also known as CERT in the formation of ceramide-enriched extracellular vesicles. Our data support a model wherein STARD11 promotes the efficient transfer of palmitate-stimulated ceramide from the ER to the MVB, where it drives the formation of ILVs. Elucidation of this fundamental pathway provides a potential target to modulate the release of extracellular vesicles in lipotoxic conditions. STARD11 may be important in other diseases associated with ceramide-dependent extracellular vesicles, a testable hypothesis.

Experimental procedures

Cells

IMH cell lines derived from IRE1α WT mice were a kind of gift of Dr. Randal Kaufman. IMH, Hepa1–6, Huh7, and HepG2 were cultured in Dulbecco's modified Eagle's medium (DMEM; Life Technologies) containing glucose (4.5 g/liter), penicillin (100 units/ml), streptomycin (100 μg/ml), and 10% fetal bovine serum (FBS). Primary mouse hepatocytes were isolated by collagenase perfusion followed by percoll purification and cultured as previously described by us (28). Greater than 95% viable isolated primary hepatocytes were plated in Waymouth's medium supplemented with 10% FBS, penicillin, and streptomycin, as above.

Extracellular vesicle isolation and characterization

Cells were grown to 90% confluency on 150-mm tissue culture dishes. The cells were washed twice with PBS to eliminate FBS-derived extracellular vesicles. Then cells were treated with either 400 μM palmitate (PA), 400 μM oleate (OA), or vehicle for 16 h in growth medium supplemented with 5% extracellular vesicle-depleted FBS, which was prepared by overnight centrifugation at 100,000 $\times$ *g* at 4 °C according to standard protocols (18) and 1% BSA. The optimal concentration and duration for cellular extracellular vesicle release prior to the onset of apoptosis in IMH and Huh7 was decided as previously described (8). Differential ultracentrifugation was used to sequentially isolate small extracellular vesicles, which we have referred to simply as extracellular vesicles throughout. Briefly, collected cell culture conditioned medium was depleted of cells and cellular debris initially by low-speed centrifugations at 2,000 $\times$ *g* for 20 min and 10,000 $\times$ *g* for 40 min. This was followed by ultracentrifugation at 100,000 $\times$ *g* for 90 min to pellet extracellular vesicles. The pellets were washed in PBS and centrifuged again at 100,000 $\times$ *g* for 90 min. The obtained extracellular vesicle pellets were resuspended in PBS or lysed in radioimmune precipitation assay buffer for downstream experiments. For each experimental condition, isolated extracellular vesicles were normalized to cell number and expressed relative to the vehicle-treated condition, unless indicated otherwise. The size distribution and concentration of isolated extracellular vesicles was assessed by nanoparticle tracking analysis as previously described by us (8). Briefly, extracellular vesicle samples were diluted in PBS at a range of concentrations between 2E+08 and 8E+08 particles/ml. Each sample was perfused through the sample chamber at a constant rate of 25 μl/min using a syringe pump. The light scatter and Brownian motion of each sample of nanoparticles was recorded at least three times, 30 s each at constant room temperature (22.5 °C); particle tracks were analyzed by NanoSight software to measure the concentration of the particles (particles/ml) and size (in nanometer). For each experimental condition, EVs isolated from equal number of cells were expressed relative to the vehicle-treated condition. For basal EV release, EV numbers were normalized to cell numbers.

Caspase 3/7 assay

Activation of caspase 3/7 is the biochemical hallmark of apoptosis (19). For caspase 3/7 assay 30,000/cm^2 IMH cells were cultured in 96-well plates. 48 h later, the cells were first pretreated with 10 μM ZVAD-FMK (Santa Cruz Biotechnology, Dallas, TX) or IDN-6556 (MedKoo Biosciences, Morrisville, NC) for 1 h followed by 400 μM palmitate or vehicle in the absence or presence of caspase inhibitors for 16 or 24 h. Equal volume of DMSO was used as control. After 16 or 24 h of treatment, respectively, apoptotic cell death was measured by Apo-ONE® homogeneous caspase-3/7 assay (Promega, Madison, WI) following the manufacturer's protocol.

Extracellular vesicles in caspase inhibitor-treated cells

IMH cells were cultured in 10-cm dishes. Approximately 90% confluent cells were treated with 10 μM of ZVAD-FMK (Santa Cruz Biotechnology) or IDN-6556 (MedKoo Biosciences, Morrisville, NC) for 1 h. Equal volume of DMSO was used as control. Before palmitate treatment, the cells were washed twice with PBS, and then the medium was changed to assay medium supplemented with palmitate or vehicle, as above, and caspase inhibitors (10 μM of ZVAD-FMK or IDN-6556). After 16 h, the medium was recovered, and sequential low-speed centrifugation was performed as described above to isolate extracellular vesicles. The extracellular vesicle pellet was resuspended in 100 μl of PBS and subjected to nanoparticle tracking analysis. For each experimental condition, isolated extracellular vesicles were normalized to cell number and expressed relative to the vehicle-treated condition.

De novo ceramide synthesis inhibitor

IMH cells were treated with vehicle or palmitate, with or without 10 μM serine palmitoyltransferase-1 inhibitor (Myriocin; Cayman Chemicals, Ann Arbor, MI) for 16 h. Extracellular vesicles were isolated and analyzed by nanoparticle tracking analysis, as described above.

Iodixanol gradient separation of extracellular vesicles

Extracellular vesicles isolated by ultracentrifugation from palmitate or vehicle-treated IMH cells (~ 200 million) were

diluted in 1.5 ml of buffer containing 0.25 M sucrose, 10 mM Tris, pH 8.0, 1 mM EDTA (pH 7.4). The solution was mixed 1:1 with 60% (w/v) stock solution of iodixanol (OptiPrep; Stemcell Technologies, Cambridge, MA). Then 3 ml of extracellular vesicle suspension was transferred to a SW55Ti rotor tube. A 40% iodixanol working solution was prepared (40% (w/v) iodixanol, 0.25 M sucrose, 10 mM Tris, pH 8.0, 1 mM EDTA, pH 7.4) and used to prepare 20 and 10% (w/v) iodixanol solutions. Next to make the gradient, 1.3 ml of 20% (w/v) iodixanol and 1.2 ml of 10% iodixanol were successively layered on top of the 3 ml of vesicle suspension, and tubes were centrifuged for 1 h at 4 °C at 350,000 × *g* in SW55Ti; 10 fractions of 490 μl were collected from the top of the tube. Density was assessed from 5 μl of each fraction using a refractometer. The remaining fractions were diluted with 4 ml of PBS and centrifuged for 30 min at 100,000 × *g* in the same rotor. These concentrated fractions were resuspended in 30 μl of PBS and subjected to nanoparticle tracking analysis. For each experimental condition, isolated extracellular vesicles were normalized to cell number and expressed relative to the vehicle-treated condition. This method was based on the protocol described by Kowal *et al.* (22).

Lipidomics

Ceramides were measured using tandem MS at Mayo Clinic Metabolomics Core Laboratory, as previously described by us (8). Extracellular vesicles isolated from equal numbers of cells treated with either vehicle, oleate, or palmitate were used to quantify changes in extracellular vesicle ceramides. Cell pellet ceramides were normalized to protein content.

Western blotting

Treated cells were collected by scraping and lysed in radioimmune precipitation assay buffer (50 mM Tris-HCl, 1% NP-40, 0.1% SDS, 150 nM NaCl, 1 mM EDTA, and 0.5% sodium deoxycholate) with protease and phosphatase inhibitors. The protein concentrations were determined by the Bio-Rad DC protein assay. Equal amounts of whole-cell lysate or protein isolated from extracellular vesicles derived from equal number of cells were loaded onto Criterion 4–15% or 12.5% Tris-HCl gel (Bio-Rad) and electrotransferred to PVDF membrane. The membranes were blocked with blocking buffer (5% nonfat milk in TBS-Tween) for 1 h at room temperature. Membranes were incubated with the following primary antibodies overnight: anti-Alix (2171; Cell Signaling); anti-STARD11 (15191-1-AP; Proteintech); anti-TSG101 (ab125011) and anti-Syntenin (ab19903) from Abcam; anti-ApoA1 (sc30089), anti-actin (sc1615), and anti-CD81 (sc166029) from Santa Cruz Biotechnology; and anti-ApoB (MABS2046) and anti-GAPDH (MAB374) from EMD Millipore Corp. Antigen-bound primary antibodies were detected with horseradish peroxidase–conjugated secondary antibodies against mouse, rabbit, or goat (Santa Cruz Biotechnology). Proteins of interest were visualized with enhanced chemiluminescence reagents (Amersham Biosciences) and HyBlot CL film (Denville Scientific Inc., Metuchen, NJ). Films were scanned using a Cannon LiDe 110 scanner and converted to grayscale in Adobe Photoshop CC 2015, and brightness and contrast were adjusted equally across the entire images.

RT–PCR and quantitative real time PCR

Total RNA was isolated by Quick-RNA MiniPrep kit (Zymo Research. Irvine, CA). Quantity and quality of RNA were assessed with a NanoDrop ND1000 (ThermoScientific, Waltham, MA), reverse transcription was performed with the iScript cDNA synthesis kit (Bio-Rad). The PCRs were performed in the Tetrad thermal cycler (MJ Research Inc., Watertown, MA) using e2TAK DNA polymerase (TaKaRa Biotechnology Inc.). The PCR-amplified fragments were analyzed with the QIAxcel advanced system (Qiagen). PCR primers used for mouse STARD11 were as follows: forward, 5′-AGTGCCTCTGACGATGTTCAC-3′, and reverse, 5′-ACCAGTTGCCAATTTGCATCA-3′. PCR primers used for human STARD11 were as follows: forward, 5′-ATGTCGGATAATCAGAGCTGGA-3′, and reverse, 5′-ATCCTGCCACCCATGAATGTA-3′. Primers for mouse hypoxanthine guanine phosphoribosyl transferase (forward, 5′-TCAGTCAACGGGGGACATAAA-3′, and reverse, 5′-GGGGCTGTACTGCTTAACCAG-3′) and human actin (forward, 5′-CATGTACGTTGCTATCCAGGC-3′, and reverse, 5′-CTCCTTAATGTCACGCACGAT-3′) were used as controls.

Immunofluorescence

The cells were grown on sterile glass coverslips in 6-well plates. The cells were fixed with 4% paraformaldehyde for 15 min, permeabilized with 0.1% Triton X-100 in PBS for 10 min, or fixed and permeabilized with ice-cold methanol for 15 min, and blocked with 5% BSA, 0.1% glycine in PBS for 30 min at room temperature. After incubating with anti-CD63 (MBS438072; MyBioSource), anti-STARD11 (PA5-28797; Thermo Fisher Scientific), anti-syntaxin6 (ab12370; Abcam), or anti-KDEL (ab50601; Abcam and sc-58774; Santa Cruz Biotechnology) antibodies diluted in blocking buffer overnight at 4 °C, the cells were washed three times with PBS, and incubated with fluorescent secondary antibodies (Alexa Fluor 350, 488, or 594; Thermo Fisher Scientific) for 1 h at room temperature protected from light. For triple immunofluorescence anti-CD63 (564221; BD Pharmingen), anti-STARD11, and anti-PDI (MA3019; Thermo Fisher Scientific) were utilized. Then after washing with PBS, coverslips were mounted in Prolong Anti-Fade (Life Technologies) on a clean glass slide.

Labeling MVBs with fluorescent lipid

The fluorescent phospholipid analog N-Rh-PE was obtained from Thermo Fisher Scientific. The cells were labeled at 4 °C with 5 μM N-Rh-PE in serum-free DMEM for 1 h. After this incubation period, the medium was removed, and cells were washed with cold serum-free DMEM to remove excess unbound lipids. After the addition of treatment medium, labeled cells were incubated for 1 h and then fixed with 4% paraformaldehyde for observation by confocal microscopy.

Proximity ligation assay

The cells were cultured on glass coverslips, fixed, and permeabilized with ice-cold methanol. The cells were incubated with anti-CD63 (sc15363; Santa Cruz Biotechnology) and anti-KDEL (sc58774; Santa Cruz Biotechnology) antibodies and pro-

cessed according to the manufacturer's protocol (Duolink PLA; Sigma). The images were observed by confocal microscope.

Labeling lysosome with LysoSensor Green

The cells were labeled with 1 μM LysoSensor Green (Thermo Fisher Scientific) into growth medium for 30 min in the incubator. The cells were washed with PBS and then fixed.

Cell transfection

For DNA transfection, IMH cells and Huh7 cells were cotransfected with GFP-tagged STARD11 (gift from Dr. Hanada), mCherry-tagged CD63 (gift from Dr. McNiven), CD-63-pEGFP (gift from Dr. Paul Luzio; Addgene plasmid 62964) using Lipofectamine LTX reagent (Invitrogen) following the manufacturer's protocol. In some experiments, transfected cells were labeled with N-Rh-PE or used for immunofluorescence.

Confocal microscopy

Fluorescence was observed with an LSM 780 confocal microscope (Zeiss) and a Plan-Apochromat 40×/1.4 oil differential interference contrast M27 objective (Zeiss). A 405-nm laser was used for the blue channel. A 488-nm laser was used for the green channel, and a 561- or 594-nm laser was used for the red channel. Images were taken at room temperature. ZEN 2.3 lite software (Zeiss) was used for acquiring images. ImageJ (National Institutes of Health) was used to analyze the raw images. The quantification shows the Pearson coefficients of colocalization. To avoid artifacts from perinuclear crowding, fluorescence pixel intensity was measured in the entire observed field rather than subcellular regions of interest. 10–20 random fields in each group were selected for quantification and statistical analysis.

Electron microscopy

Vehicle-treated IMH cells were fixed in Trump's solution (4% formaldehyde + 0.1% glutaraldehyde in 0.1 M phosphate buffer). Palmitate-treated cells were fixed in 3% glutaraldehyde and 0.1 M sodium cacodylate buffer. These cells were then processed for EM analysis using standard procedures and observed with a JEOL 1400 Plus transmission electron microscope (JEOL USA, Peabody, MA) at 80 kV.

Super-resolution microscopy

IMH cells were treated with vehicle or 400 μM palmitate for 6 h and then labeled with N-Rh-PE. For imaging of MVBs of IMH cells, the cells were incubated in treatment medium for 1 h and then fixed with 4% paraformaldehyde. Structure illumination microscopy images were captured using an Elyra PS.1 microscope (Zeiss) and a Plan-Apochromat 63×/1.4 oil differential interference contrast M27 objective (Zeiss) at room temperature.

CRISPR/Cas9 gene editing

The online tool at (http://crispr.mit.edu)[5] was used to design the single guide RNA spanning the mouse STARD11 (sgRNA, 5′-CACCGCGGCTGTCGCGTCTCCATGT-3′) and human STARD11 (sgRNA, 5′-CCGGGAATCCAGCTTGCGTCG-ACA-3′ and 5′-CCGGTAATCAGAGCTGGAACTCGT-3′). Annealed oligonucleotides of sgRNA were used to generate a lentivirus following subcloning into the lentiCRISPRv1 plasmid (Addgene) and transfected into HEK293T cells using Lipofectamine LTX reagent, as previously described by us (8). Virus was harvested at 48 h after transfection, and IMH cells were infected with STARD11 targeting lentivirus in the presence of 8 μg/ml Polybrene. Infected cells were selected under 4 μg/ml blasticidin (InvivoGen) selection pressure. STARD11 knockout cell lines in Huh7 cells were created by Guide-it CRISPR/Cas9 system (TaKaRa Biotechnology Inc.) according to the manufacturer's instruction.

Quantitation of apoptosis and cytotoxicity

IMH cells were stained with 4′,6-diamidino-2-phenylindole for 5 min and visualized using fluorescent microscope to count number of apoptotic nuclei. IMH WT and STARD11$^{-/-}$ cells were plated in 96-well plates. The cells were then treated with 400 μM palmitate. After 16 and 20 h of treatment, cell viability was measured by WST-1 assay (Sigma–Aldrich) per the manufacturer's instructions.

Statistical and data analyses

The data represent the means ± S.E. from three or more experiments unless indicated. Two-tailed Student's *t* test was used for comparing groups. Statistical analyses were performed in GraphPad Prism version 6.00 for Windows (GraphPad Software, La Jolla, CA). A p value of <0.05 was considered significant.

Author contributions—M. F., A. S. M., K. N., and H. M. conceptualization; M. F. data curation; M. F. software; M. F., D. D., and H. M. formal analysis; M. F. validation; M. F., D. D., A. S. M., and E.K. investigation; M. F. visualization; M. F. methodology; M. F. and H. M. writing-original draft; M. F. and H. M. project administration; M. F., D. D., A. S. M., and H. M. writing-review and editing; A. S. M., K. N., and H. M. supervision; H. M. funding acquisition.

Acknowledgments—We are grateful to Dr. Gregory J. Gores for critical review of the manuscript and Dr. Kentaro Hanada for the gift of GFP-hCERT. CD63–mCherry was a gift from Dr. Mark McNiven, and CD63–GFP was from Addgene. We are also grateful to Dr. David Katzmann and Dr. Brian Davies for useful discussions and insight into MVB formation, and Courtney Hoover for outstanding administrative support. The optical microscopy core of the Mayo Clinic Center for Cell Signaling was supported by Grant P30DK084567 from the NIDDK, National Institutes of Health. The Mayo Clinic Metabolomics Core was supported by Grants U24DK100469 and UL1TR000135 from the NIDDK, National Institutes of Health.

References

1. Hirsova, P., Ibrahim, S. H., Verma, V. K., Morton, L. A., Shah, V. H., LaRusso, N. F., Gores, G. J., and Malhi, H. (2016) Extracellular vesicles in liver pathobiology: small particles with big impact. *Hepatology* **64,** 2219–2233 CrossRef Medline

[5] Please note that the JBC is not responsible for the long-term archiving and maintenance of this site or any other third party hosted site.

2. Verma, V. K., Li, H., Wang, R., Hirsova, P., Mushref, M., Liu, Y., Cao, S., Contreras, P. C., Malhi, H., Kamath, P. S., Gores, G. J., and Shah, V. H. (2016) Alcohol stimulates macrophage activation through caspase-dependent hepatocyte derived release of CD40L containing extracellular vesicles. *J. Hepatol.* **64,** 651–660 CrossRef Medline
3. Kalluri, R. (2016) The biology and function of exosomes in cancer. *J. Clin. Invest.* **126,** 1208–1215 CrossRef Medline
4. Costa-Silva, B., Aiello, N. M., Ocean, A. J., Singh, S., Zhang, H., Thakur, B. K., Becker, A., Hoshino, A., Mark, M. T., Molina, H., Xiang, J., Zhang, T., Theilen, T. M., García-Santos, G., Williams, C., *et al.* (2015) Pancreatic cancer exosomes initiate pre-metastatic niche formation in the liver. *Nat. Cell Biol.* **17,** 816–826 CrossRef Medline
5. Raposo, G., and Stoorvogel, W. (2013) Extracellular vesicles: exosomes, microvesicles, and friends. *J. Cell Biol.* **200,** 373–383 CrossRef Medline
6. Trajkovic, K., Hsu, C., Chiantia, S., Rajendran, L., Wenzel, D., Wieland, F., Schwille, P., Brügger, B., and Simons, M. (2008) Ceramide triggers budding of exosome vesicles into multivesicular endosomes. *Science* **319,** 1244–1247 CrossRef Medline
7. de Almeida, I. T., Cortez-Pinto, H., Fidalgo, G., Rodrigues, D., and Camilo, M. E. (2002) Plasma total and free fatty acids composition in human non-alcoholic steatohepatitis. *Clin. Nutr.* **21,** 219–223 CrossRef Medline
8. Kakazu, E., Mauer, A. S., Yin, M., and Malhi, H. (2016) Hepatocytes release ceramide-enriched pro-inflammatory extracellular vesicles in an IRE1α-dependent manner. *J. Lipid Res.* **57,** 233–245 CrossRef Medline
9. Levy, M., and Futerman, A. H. (2010) Mammalian ceramide synthases. *IUBMB Life* **62,** 347–356 Medline
10. Kowal, J., Tkach, M., and Théry, C. (2014) Biogenesis and secretion of exosomes. *Curr. Opin. Cell Biol.* **29,** 116–125 CrossRef Medline
11. Stuffers, S., Sem Wegner, C., Stenmark, H., and Brech, A. (2009) Multivesicular endosome biogenesis in the absence of ESCRTs. *Traffic* **10,** 925–937 CrossRef Medline
12. Theos, A. C., Truschel, S. T., Tenza, D., Hurbain, I., Harper, D. C., Berson, J.F., Thomas, P.C., Raposo, G., and Marks, M.S. (2006) A lumenal domain-dependent pathway for sorting to intralumenal vesicles of multivesicular endosomes involved in organelle morphogenesis. *Dev. Cell* **10,** 343–354 CrossRef Medline
13. Matsuo, H., Chevallier, J., Mayran, N., Le Blanc, I., Ferguson, C., Fauré, J., Blanc, N. S., Matile, S., Dubochet, J., Sadoul, R., Parton, R. G., Vilbois, F., and Gruenberg, J. (2004) Role of LBPA and Alix in multivesicular liposome formation and endosome organization. *Science* **303,** 531–534 CrossRef Medline
14. Hanada, K., Kumagai, K., Yasuda, S., Miura, Y., Kawano, M., Fukasawa, M., and Nishijima, M. (2003) Molecular machinery for non-vesicular trafficking of ceramide. *Nature* **426,** 803–809 CrossRef Medline
15. Kawano, M., Kumagai, K., Nishijima, M., and Hanada, K. (2006) Efficient trafficking of ceramide from the endoplasmic reticulum to the Golgi apparatus requires a VAMP-associated protein-interacting FFAT motif of CERT. *J. Biol. Chem.* **281,** 30279–30288 CrossRef Medline
16. Tsujishita, Y., and Hurley, J. H. (2000) Structure and lipid transport mechanism of a StAR-related domain. *Nat. Struct. Biol.* **7,** 408–414 CrossRef Medline
17. Alpy, F., and Tomasetto, C. (2005) Give lipids a START: the StAR-related lipid transfer (START) domain in mammals. *J. Cell Sci.* **118,** 2791–2801 CrossRef Medline
18. Thery, C., Amigorena, S., Raposo, G., and Clayton, A. (2006) Isolation and characterization of exosomes from cell culture supernatants and biological fluids. *Curr. Protoc. Cell Biol.* Chapter 3, Unit 3.22 CrossRef Medline
19. Malhi, H., Bronk, S. F., Werneburg, N. W., and Gores, G. J. (2006) Free fatty acids induce JNK-dependent hepatocyte lipoapoptosis. *J. Biol. Chem.* **281,** 12093–12101 CrossRef Medline
20. Malhi, H., Barreyro, F. J., Isomoto, H., Bronk, S. F., and Gores, G. J. (2007) Free fatty acids sensitise hepatocytes to TRAIL mediated cytotoxicity. *Gut* **56,** 1124–1131 CrossRef Medline
21. Zhang, J., Reedy, M. C., Hannun, Y. A., and Obeid, L. M. (1999) Inhibition of caspases inhibits the release of apoptotic bodies: Bcl-2 inhibits the initiation of formation of apoptotic bodies in chemotherapeutic agent-induced apoptosis. *J. Cell Biol.* **145,** 99–108 CrossRef Medline
22. Kowal, J., Arras, G., Colombo, M., Jouve, M., Morath, J. P., Primdal-Bengtson, B., Dingli, F., Loew, D., Tkach, M., and Théry, C. (2016) Proteomic comparison defines novel markers to characterize heterogeneous populations of extracellular vesicle subtypes. *Proc. Natl. Acad. Sci. U.S.A.* **113,** E968–E977 CrossRef Medline
23. Pickersgill, L., Litherland, G. J., Greenberg, A. S., Walker, M., and Yeaman, S. J. (2007) Key role for ceramides in mediating insulin resistance in human muscle cells. *J. Biol. Chem.* **282,** 12583–12589 CrossRef Medline
24. Ghossoub, R., Lembo, F., Rubio, A., Gaillard, C. B., Bouchet, J., Vitale, N., Slavík, J., Machala, M., and Zimmermann, P. (2014) Syntenin-ALIX exosome biogenesis and budding into multivesicular bodies are controlled by ARF6 and PLD2. *Nat. Commun.* **5,** 3477 CrossRef Medline
25. Loewen, C. J., Roy, A., and Levine, T. P. (2003) A conserved ER targeting motif in three families of lipid binding proteins and in Opi1p binds VAP. *EMBO J.* **22,** 2025–2035 CrossRef Medline
26. Levine, T. P., and Munro, S. (2002) Targeting of Golgi-specific pleckstrin homology domains involves both PtdIns 4-kinase-dependent and -independent components. *Curr. Biol.* **12,** 695–704 CrossRef Medline
27. Sugiki, T., Takeuchi, K., Yamaji, T., Takano, T., Tokunaga, Y., Kumagai, K., Hanada, K., Takahashi, H., and Shimada, I. (2012) Structural basis for the Golgi association by the pleckstrin homology domain of the ceramide trafficking protein (CERT). *J. Biol. Chem.* **287,** 33706–33718 CrossRef Medline
28. Faubion, W. A., Guicciardi, M. E., Miyoshi, H., Bronk, S. F., Roberts, P. J., Svingen, P. A., Kaufmann, S. H., and Gores, G. J. (1999) Toxic bile salts induce rodent hepatocyte apoptosis via direct activation of Fas. *J. Clin. Invest.* **103,** 137–145 CrossRef Medline
29. Friedman, J. R., Dibenedetto, J. R., West, M., Rowland, A. A., and Voeltz, G. K. (2013) Endoplasmic reticulum-endosome contact increases as endosomes traffic and mature. *Mol. Biol. Cell* **24,** 1030–1040 CrossRef Medline
30. Munro, S., and Pelham, H. R. (1987) A C-terminal signal prevents secretion of luminal ER proteins. *Cell* **48,** 899–907 CrossRef Medline
31. Savina, A., Fader, C. M., Damiani, M. T., and Colombo, M. I. (2005) Rab11 promotes docking and fusion of multivesicular bodies in a calcium-dependent manner. *Traffic* **6,** 131–143 CrossRef Medline
32. Willem, J., ter Beest, M., Scherphof, G., and Hoekstra, D. (1990) A non-exchangeable fluorescent phospholipid analog as a membrane traffic marker of the endocytic pathway. *Eur J. Cell Biol.* **53,** 173–184 Medline
33. Savina, A., Furlán, M., Vidal, M., and Colombo, M. I. (2003) Exosome release is regulated by a calcium-dependent mechanism in K562 cells. *J. Biol. Chem.* **278,** 20083–20090 CrossRef Medline
34. Hanada, K. (2014) Co-evolution of sphingomyelin and the ceramide transport protein CERT. *Biochim. Biophys. Acta* **1841,** 704–719 CrossRef Medline
35. Kaiser, S. E., Brickner, J. H., Reilein, A. R., Fenn, T. D., Walter, P., and Brunger, A. T. (2005) Structural basis of FFAT motif-mediated ER targeting. *Structure* **13,** 1035–1045 CrossRef Medline
36. Obata, Y., Kita, S., Koyama, Y., Fukuda, S., Takeda, H., Takahashi, M., Fujishima, Y., Nagao, H., Masuda, S., Tanaka, Y., Nakamura, Y., Nishizawa, H., Funahashi, T., Ranscht, B., Izumi, Y., *et al.* (2018) Adiponectin/T-cadherin system enhances exosome biogenesis and decreases cellular ceramides by exosomal release. *JCI Insight* **3**
37. Kumagai, K., Kawano-Kawada, M., and Hanada, K. (2014) Phosphoregulation of the ceramide transport protein CERT at serine 315 in the interaction with VAMP-associated protein (VAP) for inter-organelle trafficking of ceramide in mammalian cells. *J. Biol. Chem.* **289,** 10748–10760 CrossRef Medline
38. Faubion, W. A., Guicciardi, M. E., Miyoshi, H., Bronk, S. F., Roberts, P. J., Svingen, P. A., Kaufmann, S. H., and Gores, G. J. (1999) Toxic bile salts induce rodent hepatocyte apoptosis via direct activation of Fas. *J. Clin. Invest.* **103,** 137–145 CrossRef Medline
39. Thery, C., Amigorena, S., Raposo, G., and Clayton, A. (2006) Isolation and characterization of exosomes from cell culture supernatants and biological fluids. *Curr. Protoc. Cell Biol.* Chapter 3, Unit 3.22 CrossRef Medline

StAR-related lipid transfer domain 11 (STARD11)–mediated ceramide transport mediates extracellular vesicle biogenesis

Masanori Fukushima, Debanjali Dasgupta, Amy S. Mauer, Eiji Kakazu, Kazuhiko Nakao and Harmeet Malhi

J. Biol. Chem. 2018, 293:15277-15289.
doi: 10.1074/jbc.RA118.002587 originally published online August 23, 2018

STARD11-mediated ceramide transport mediates extracellular vesicle biogenesis

Masanori Fukushima, Debanjali Dasgupta, Amy S. Mauer, Eiji Kakazu, Kazuhiko Nakao, and Harmeet Malhi

List of Supporting Information

Supporting Information Figure 1

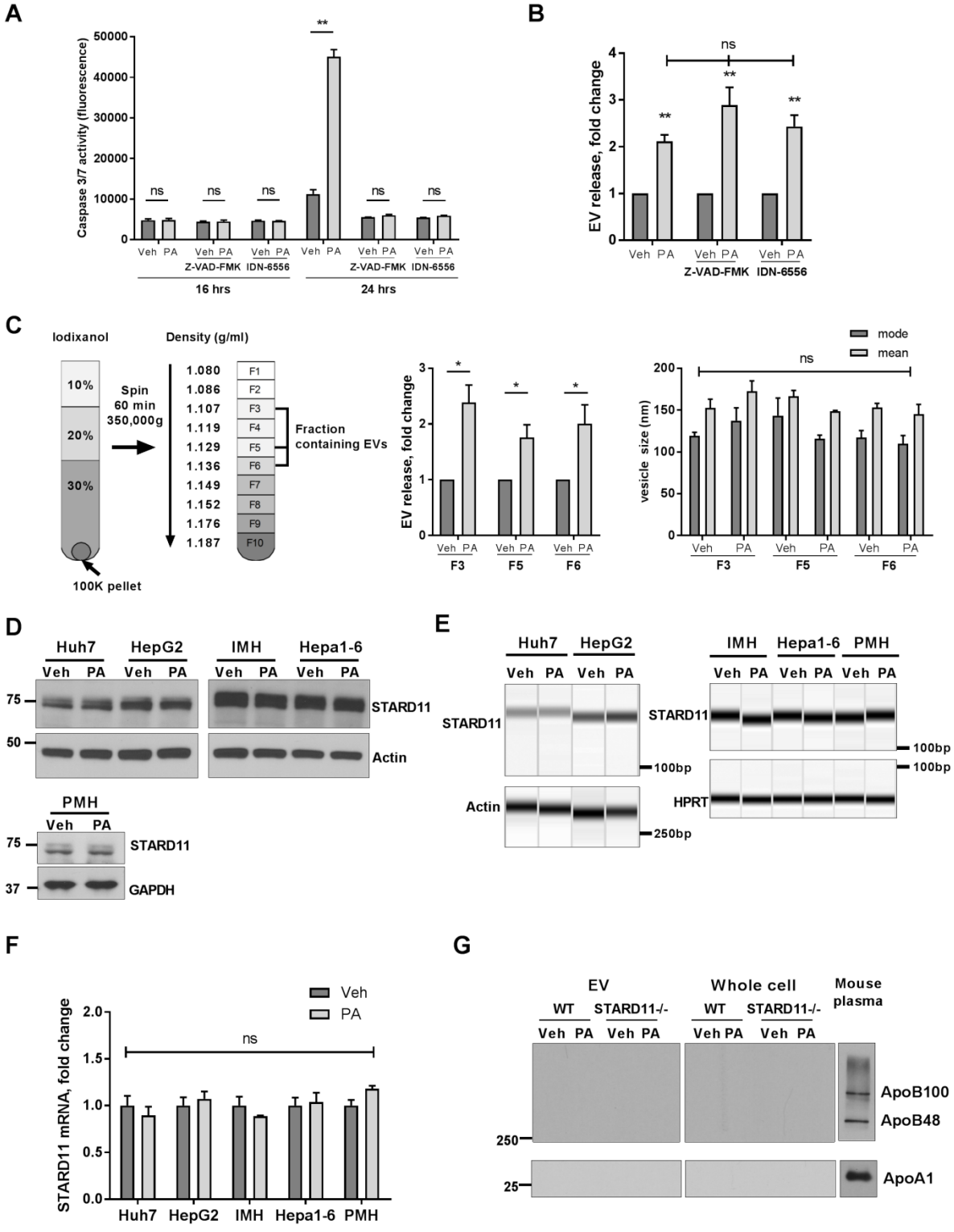

Supporting Information Figure 1. Characterization of lipotoxic extracellular vesicles and STARD11 expression. (A) Immortalized mouse hepatocyte (IMH) cells were treated with vehicle or 400 μM palmitate (PA), with or without apoptotic inhibitors (10 μM Z-VAD-FMK, 10 μM IDN-6556) for 16 hours. Apoptosis was assessed by caspase 3/7 assay. (B) EV release in IMH cells treated with vehicle or 400 μM PA, with or without apoptotic inhibitors. (C) EV pellets were separated into ten fractions by iodixanol gradient. Densities of recovered fractions were displayed in the cartoon. Ten fractions were collected and analyzed by nanoparticle tracking analysis. The number and size of EVs from three fractions (F3,5,6), which could observe particles, were measured by nanoparticle tracking analysis. (D) STARD11 protein was confirmed by western blotting in Huh7, HepG2, immortalized mouse hepatocyte (IMH), Hepa1-6 and primary mouse hepatocyte (PMH). Cells were treated with vehicle or 400 μM PA for 8 hours. (E, F) STARD11 mRNA abundance was assessed by RT-PCR. Human actin and mouse HPRT were used as a control. PCR fragments were resolved by capillary electrophoresis. The intensity is indicated as bar graphs. (G) EVs isolated from equal number of cells and cell lysates from IMH cell line were analyzed by western blot. Mouse plasma was used as a positive control for apolipoproteins A1, B48 and B100. *, $P < 0.05$, **, $P < 0.01$, ns, not significant. All error bars are SEM. These data were obtained from three or more independent experiments.

Supporting Information Figure 2

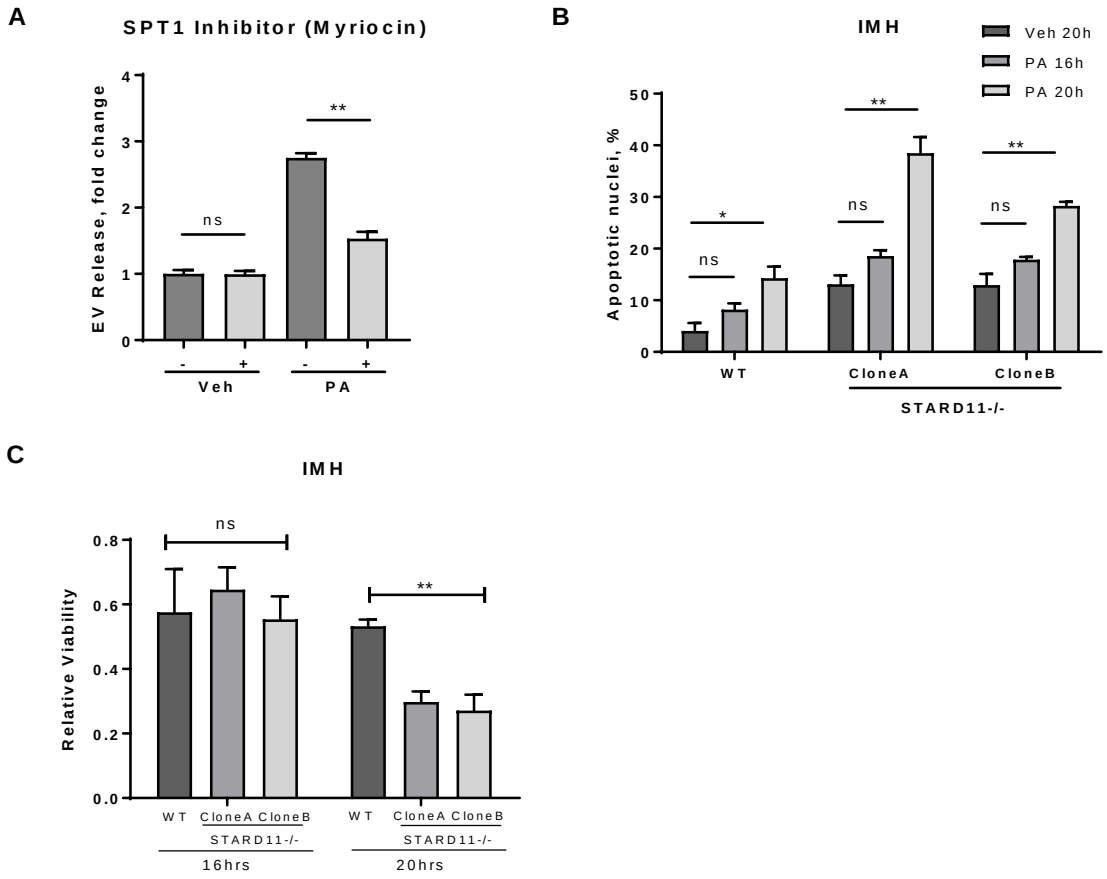

Supporting Information Figure 2. STARD11-mediated ceramide transport mitigates palmitate-induced cytotoxicity. (A) EVs were isolated from immortalized mouse hepatocyte (IMH) cells were treated with vehicle or 400 μM palmitate (PA), with or without 10 μM serine palmitoyltransferase-1inhibitor (Myriocin). (B) IMH wildtype (WT), STARD11 knock out (STARD11-/-) clone A and B cells were treated with vehicle or 400 μM PA for 16 hours or 20 hours. Apoptosis was assessed by DAPI staining and counting of apoptotic nuclei. (C) IMH WT, STARD11-/- clone A and B cells were treated with vehicle or 400 μM PA for 16 hours or 20 hours. Cell viability was measured by WST-1 assay. *, $P < 0.05$, **, $P < 0.01$, ns, not significant. All error bars are SEM. These data were obtained from three or more independent experiments.

Supporting Information Figure 3

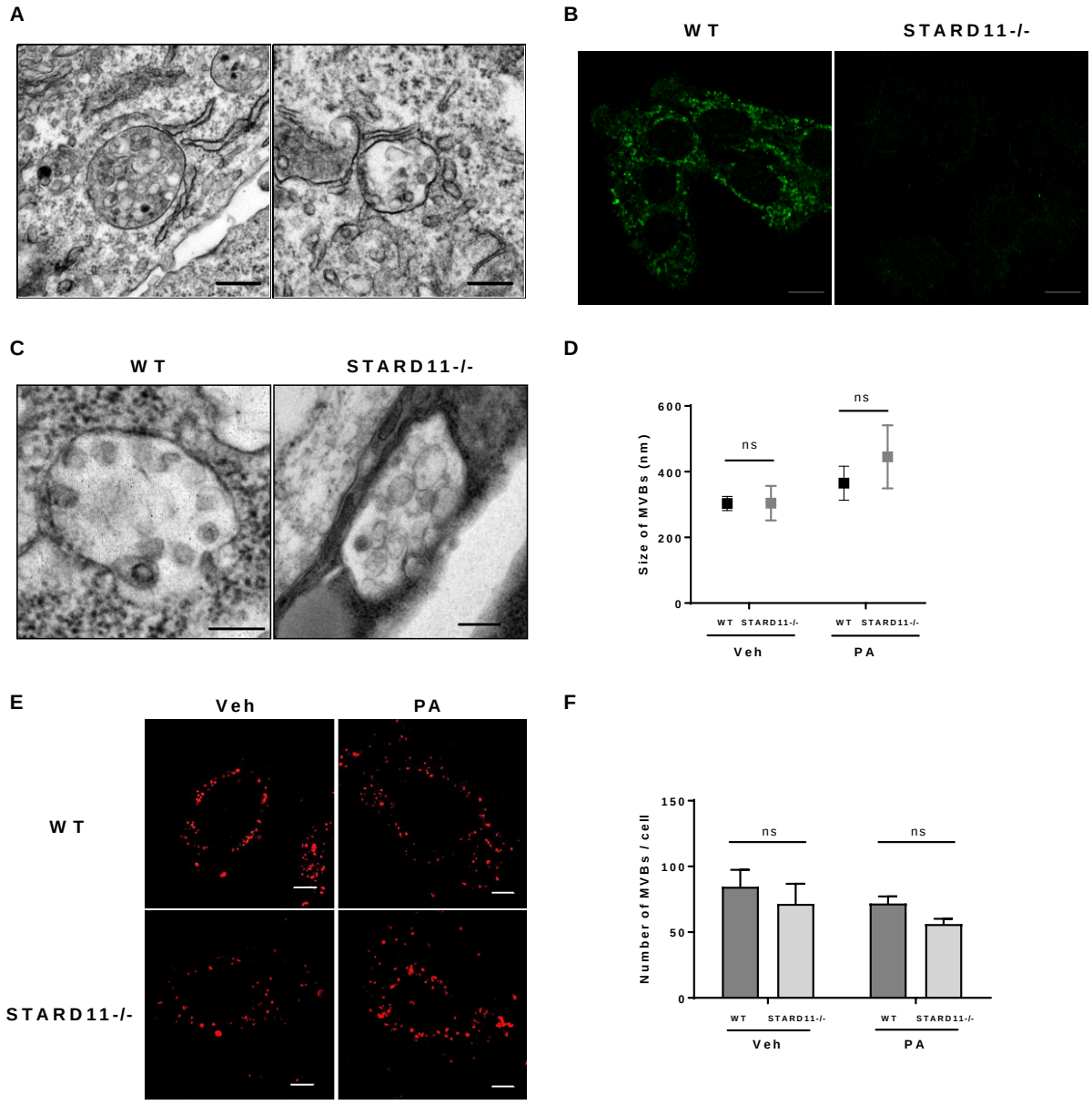

Supporting Information Figure 3. MVB size and number are comparable in WT and STARD11-/- cells. (A) Representative electron micrographs (EM) of the MVB of immortalized mouse hepatocyte (IMH) showing endoplasmic reticulum within 30 nm of the MVB. The scale bars are 200 nm. (B) IMH wildtype (WT) and STARD11 knock out (STARD11-/-) cells were labeled with anti-STARD11 antibody by immunofluorescence. The scale bars indicate 10 μm. (C, D) Representative EM images of the MVB of IMH-WT and IMH-STARD11-/- and quantification of the size of MVBs. The scale bars are 200 nm. (E, F) Representative super resolution structured illumination microscopy images of MVBs and quantification of the number of MVBs per cell. The scale bars are 5 μm. ns, not significant. All error bars are SEM. These data were obtained three or more independent experiments.